

Negative spin Hall magnetoresistance in epitaxial antiferromagnetic NiO(001)/Pt thin films

L. Baldrati^{1,2}, A. Ross^{1,2}, T. Niizeki³, R. Ramos³, J. Cramer^{1,2}, O. Gomonay¹, E. Saitoh^{3,4,5,6}, J. Sinova¹, M. Kläui^{1,2*}

¹*Institute of Physics, Johannes Gutenberg-University Mainz, 55128 Mainz, Germany*

²*Graduate School of Excellence Materials Science in Mainz, 55128 Mainz, Germany ,*

³*Advanced Institute for Materials Research, Tohoku University, Sendai 980-8577, Japan*

⁴*Institute for Materials Research, Tohoku University, Sendai 980-8577, Japan*

⁵*Advanced Science Research Center, Japan Atomic Energy Agency, Tokai 319-1195, Japan*

⁶*Center for Spintronics Research Network, Tohoku University, Sendai 980-8577, Japan*

**Electronic Mail: klaeui@uni-mainz.de*

ABSTRACT

We report the observation of negative spin Hall magnetoresistance in a thin film of epitaxial antiferromagnetic NiO, without any ferromagnetic elements. The angular dependence of the magnetoresistance was measured in magnetic fields up to 11 T, using both in-plane and out-of-plane angular scans. The onset of the SMR signal occurs between 1 and 3 T and no saturation is visible up to 11 T. The sign of the SMR is consistent with recent theoretical predictions and our results can be explained by a model considering the field-induced redistribution of S-domains, competing with the destressing energy arising from the interaction of the magnetostrictive NiO layer with the nonmagnetic MgO substrate. From the observed SMR ratio, we estimate the spin mixing conductance at the NiO/Pt interface to be greater than $2 \times 10^{14} \Omega^{-1} \text{ m}^{-2}$, comparable to early works on YIG/Pt systems. Our results highlight the presence of negative SMR in antiferromagnetic thin films, confirming the existence of efficient spin transport and suggesting the possibility of an electrical detection of the Néel vector in this class of materials, even for thin films relevant for applications.

Manuscript

Antiferromagnets are materials with compensated magnetic sublattices, free from stray fields, robust against external magnetic perturbations and potentially operating at THz frequencies.^{1,2} In heavy metal/ferrimagnetic insulator (HM/FMI) bilayers, a magnetoresistance effect caused by the interconversion between an electric current and a spin current via the spin Hall effect (SHE) and inverse spin Hall effect (ISHE) has been first observed in YIG/Pt, the so-called spin Hall magnetoresistance (SMR).³⁻⁵ In antiferromagnetic insulators, where no anisotropic magnetoresistance can be detected,⁶ SMR provides information on the orientation of the Néel vector,⁷ which otherwise requires X-ray magnetic linear dichroism (XMLD) in synchrotrons.⁸ If SMR follows the same angular dependence as YIG/Pt bilayers, it is considered positive by convention,⁴ whilst negative when the maximum of the resistance is shifted by 90° as a function of the magnetic field \mathbf{H} . This can occur in antiferromagnets,⁷ since the Néel vector \mathbf{N} tends to align orthogonal to \mathbf{H} , due to the higher magnetic susceptibility in this direction. The sign of SMR in antiferromagnets is not fully clarified. Both positive and negative SMR have been observed in HM/antiferromagnetic insulator(AFMI)/FM trilayers,⁹⁻¹³ where the spin backflow from the antiferromagnet and the FMI is detected. A non-monotonic behavior of the SMR as a function of the AFM thickness,^{10,12} and a change of sign as a function of temperature have been reported in AFMs,⁹⁻¹² and in compensated ferrimagnets,¹⁴ suggesting a competition between positive and negative contributions, arising from the FMI and the AFMI, respectively. SMR in bilayers of antiferromagnets/HM has been investigated only very recently. Positive SMR was observed in bilayers of SrMnO₃ and Pt,¹⁵ possibly due to a small canted/uncompensated magnetization \mathbf{M} .¹⁶ A report on negative SMR in a NiO(111) bulk crystal/Pt bilayer, where the magnetic field rotates in the NiO (111) easy plane,¹⁷ in agreement with theoretical predictions,⁷ was published during the preparation of this work. At present, spin Hall magnetoresistance in NiO(001) thin films, the most stable NiO orientation,¹⁸ has not been reported yet, nor it is clear how SMR can occur in epitaxial thin films, relevant for applications, or when the magnetic field

is rotated in a NiO plane other than the (111) magnetic easy planes. In this paper, we fill these gaps, by showing the occurrence of SMR in a bilayer of Pt and epitaxial NiO(001) thin films grown on MgO(001) substrates by sputtering, fitting our results with a simple model based on the competition between Zeeman energy and destressing energy from the substrate.¹⁹ Finally, from the measured data, we gauge the efficiency of the spin transport in antiferromagnetic thin films, by estimating the spin mixing conductance of the NiO(001)/Pt interface.⁵

NiO is an easy-plane, collinear antiferromagnetic insulator with a band gap of 4 eV and a bulk Néel temperature of 573K.²⁰ Above the Néel temperature, NiO exhibits a cubic rock salt structure, while the unit cell contracts along one of the four [111] directions in the bulk antiferromagnetic state.²¹ Within each of these four magnetostrictive domains (T-domains), the spins are confined to ferromagnetic (111) planes, which in turn are antiferromagnetically ordered.^{21–23} The spins are relatively free to rotate to point in one of the three $[11\bar{2}]$ directions, leading to three possible independent spin domains (S-domains) within each of the T-domains. Like T-domains, S-domains also possess different strains of magnetoelastic origin. The magnetic structure of NiO, for a single S-domain, is shown in Fig. 1a. With the application of an external field, the main mechanism of spin realignment is the motion of the AFM domain walls,^{21,23–25} which was reported to occur between <1 T and 7 T for bulk crystals.^{24–27}

The investigated NiO thin films of 90 nm thickness were grown on a (001)-oriented MgO substrate by means of radio frequency (RF) reactive magnetron sputtering. Epitaxial growth of NiO stems from the small lattice mismatch of ~1% between NiO ($a_{\text{NiO}} = 4.176 \text{ \AA}$) and MgO ($a_{\text{MgO}} = 4.212 \text{ \AA}$), both exhibiting a rock salt structure. The samples were grown in a sputtering system QAM4 by ULVAC, at a base pressure of 10^{-5} Pa. The MgO substrates were pre-annealed at 800 °C for 2h. Subsequently, the NiO films were deposited from a Ni target in a steady Argon (15 sccm) and Oxygen (4.2 sccm) flow at 450 °C. Finally, a Pt top layer ($d_{\text{Pt}} = 7.5 \text{ nm}$) for the SMR experiment was deposited in-situ, after cooling down the samples to room temperature in

vacuum. Epitaxial growth of the NiO(001) films was checked by X-ray diffraction and reciprocal space mapping, as detailed elsewhere.²⁸

The NiO/Pt bilayers were patterned into Hall bars, using electron beam lithography and ion beam etching. The Hall bar geometry comprises a 75 μm x 650 μm sized main strip and four 20 μm x 100 μm contact strips, symmetrically arranged at a distance of 550 μm . The samples were installed in a variable temperature insert cryostat with a superconducting magnet, and static magnetic fields of up to 11 T were applied. The sample was rotated through the xy and yz planes (Figs. 1b,c), by means of a piezoelectric rotator ANRv51RES from Attocube, operated in an open loop. While rotating the sample, a charge current from a Keithley 2400 was passed through the Hall bar and the transverse and longitudinal resistance were simultaneously captured with two Keithley 2182A nanovoltmeters. The sample was rotated clockwise by 180° degrees, then the field was reversed and the sample was rotated counter-clockwise to the initial position. The longitudinal and transverse resistance were calculated as the average sum and difference, respectively, of positive and negative currents. Drifts in the resistance occurring during the reversal of the field were corrected by summing a constant offset to the backward part, in order to ensure the continuity of the resistance. Linear drifts due to a non-perfect temperature stabilization were corrected when detected. The sample temperature was maintained at 199.46±0.02K for all measurements, as probed by a Cernox-1050 sensor by Lakeshore.

The angular dependence of the MR amplitude for external fields \mathbf{H} of 1 T, 5 T and 11 T rotated in the xy and yz planes are shown in Figs. 2a,b and 2c,d respectively. In YIG/NiO/Pt trilayers, the NiO has been shown to suppress the magnetic proximity effect in the Pt layer,⁹ therefore we can exclude the presence of standard AMR and attribute the observed variation to SMR. The longitudinal (R_{xx}) and transverse (R_{xy}) resistances measured in the xy-plane scan were respectively fitted with a $\sin^2(\alpha + \alpha_{0,xx})$ and $\sin^2(\alpha + \alpha_{0,xy})$ functions (the fit is shown as continuous lines), where $\alpha_{0,xx}$ and $\alpha_{0,xy}$ are constants. In Fig. 2b it is possible to distinguish a

$\sin(\alpha)$ Hall signal with 360° period, arising from a small out-of-plane component of field B_z due to misalignment.¹⁷ The small differences of the offsets $\alpha_{0,xx} = 6^\circ \pm 2^\circ$ and $\alpha_{0,xy} = -40^\circ \pm 2^\circ$, to the respectively expected values of 0° and -45° , are likely to be due to a non-corrected misalignment of the direction of the current, while their difference $\alpha_{0,xx} - \alpha_{0,xy} = 46 \pm 3^\circ$ is in agreement to what is expected for SMR. For the yz plane, the transverse signal is dominated by the ordinary Hall effect of the Pt top layer, which is linear with the field and follows a $-\cos(\beta + \beta_{0,\text{Hall}})$ functional angular dependence. By correcting the offset in order to set $\beta_{0,\text{Hall}} = 0^\circ$, and applying the same correction to the transverse and longitudinal data, we find that the longitudinal resistance is modulated with a $\sin^2(\beta + \beta_{0,xx})$ dependence, where surprisingly $\beta_{0,xx} = 31^\circ \pm 3^\circ$ has a finite value. In this plane, a small contribution from ordinary magnetoresistance may also be present.²⁹ Finally, the MR amplitude as a function of field for the xy plane is shown in Fig. 3. The longitudinal and transverse MR amplitudes increase with the field, showing no saturation, and are in good agreement with each other, if the geometric scaling factor of 8.67, calculated as the ratio between the length and width of the Hall bar, is taken into account.

The data presented in Fig. 2 show a negative sign of the SMR, in agreement with theoretical predictions,⁷ and resulting from a component of the Néel vector perpendicular to the field. As shown in Fig. 1a, due to the SHE, a charge current passed through the HM layer causes a transverse spin current, polarized in plane, to flow across the Pt/NiO interface, leading to a spin accumulation μ_s . Within the xy plane, the longitudinal resistance of the Pt is highest when the external field $\mathbf{H} \parallel \mu_s$, and minimized for $\mathbf{H} \perp \mu_s$. In ferromagnets exhibiting a net magnetization \mathbf{M} , the main component of the polarization of the spin current flowing along z is proportional to $\mathbf{M} \times (\mathbf{M} \times \mu_s)$,⁵ where μ_s is the polarization of the spin accumulation from the SHE. When $\mathbf{M} \parallel \mu_s$, the spin current is reflected from the magnetic material,^{4,14} and the additional charge current induced by the conversion of the reflected spin current via the ISHE lowers the resistance. The spin current is instead absorbed by spin transfer torque if $\mu_s \perp \mathbf{M}$, yielding a state of higher resistance in the HM. As a result, as the angle between the current and magnetic

field is changed, a $\cos^2(\alpha)$ modulation of the resistance is obtained.⁴ By contrast, in antiferromagnets the magnetic moments follow the Néel vector \mathbf{N} , therefore the main component of the polarization of the spin current flowing along z is proportional to $\mathbf{N} \times (\mathbf{N} \times \boldsymbol{\mu}_s)$.^{4,7} Note that the configuration of lowest Zeeman energy is the one having $\mathbf{N} \perp \mathbf{H}$,²⁴ therefore the dependence of the SMR versus the field is shifted by 90° , yielding the $\sin^2(\alpha)$ dependence found here. The sign of the observed SMR is therefore consistent with theoretical predictions,⁷ and with the negative sign of the SMR found in YIG/NiO/Pt trilayers^{9,11,12} and in NiO(111)/Pt single bulk crystals.¹⁷

The field dependence and the offset found in the yz -planes can be explained by a model taking into account elastic effects and the Zeeman energy, computed as $(\mathbf{NH})^2/H_{\text{exch}}$, where H_{exch} parametrizes the exchange interaction between the magnetic sublattices. Below the Néel temperature, S-domains with different orientations of the Néel vector have different strains, due to the pronounced magnetoelastic interactions in NiO,³⁰ which are incompatible with the non-deformed nonmagnetic substrate and produce mechanical stresses in the sample. The macroscopic component of the stresses can be relaxed in the presence of a domain structure with zero average strain. We model this effect by introducing the destressing energy,^{6,19} which is proportional to $H_{\text{destr}}[\langle N_x^2 - N_y^2 \rangle^2 + 4\langle N_x N_y \rangle^2]$, where $\langle \rangle$ denotes the average. The value of the destressing field H_{destr} depends on the properties of the interface between NiO and the nonmagnetic substrate. Within this model the domain structure is described by the relative fraction of different domains which, in assumption of movable domain walls, could be considered as variables. Our calculations show that the effect of the external magnetic field, which removes the degeneracy of different S-domains, is partially screened by the domain redistribution. For in-plane field and a single (111) T-domain, the $[\bar{2}11]$ and $[1\bar{2}1]$ S-domains compete, yielding a contribution into the longitudinal and transverse components of the resistance of the type:

$$\frac{\Delta R_{xx}(\alpha)}{\bar{R}} = \left(\frac{\Delta\rho}{\rho}\right) \frac{H^2}{H_{exch}H_{destr}} \sin^2(\alpha) \quad (1)$$

$$\frac{\Delta R_{xy}(\alpha)}{\bar{R}} = \left(\frac{\Delta\rho}{\rho}\right) \frac{H^2}{2H_{exch}H_{destr}} \sin(2\alpha) \quad (2)$$

where $\Delta\rho/\rho$ is the SMR value defined below (see Eq.(5)). Note that the longitudinal and transverse components are shifted by 45° , which agrees well with the measurements in Fig. 2a,b, as was discussed above. The field applied in yz plane induces redistribution of all three types of domains: $[\bar{2}11]$, $[1\bar{2}1]$ and $[11\bar{2}]$. In this case

$$\frac{\Delta R_{xx}(\beta)}{\bar{R}} = \left(\frac{\Delta\rho}{\rho}\right) \frac{\sqrt{5}H^2}{2H_{exch}H_{destr}} \sin^2(\beta + \beta_{0,xx}) \quad (3)$$

$$\frac{\Delta R_{xy}(\beta)}{\bar{R}} = \left(\frac{\Delta\rho}{\rho}\right) \frac{\sqrt{10}H^2}{4H_{exch}H_{destr}} \sin[2(\beta + \beta_1)] \quad (4)$$

Where $\beta_{0,xx} \sim 26.8^\circ$ and $\beta_1 \sim 18.5^\circ$. The experimental dependences are shown in Fig. 2c,d and the fit from the experiments yields a value of $\beta_{0,xx} = 31^\circ \pm 3^\circ$, matching well the predictions of our model. Moreover, we can extract from the model a quadratic field dependence of the amplitude of SMR signal up to the monodomainization field $H_{MD} = \sqrt{2H_{exch}H_{destr}}$, at which all the unfavourable domains are swept out from the sample and the Néel vector is oriented perpendicular to the field direction. Above this field, the SMR signal saturates and does not depend on \mathbf{H} . In our experiments no saturation of the signal up to 11 T is observed, however the field dependence is in agreement with our data, as shown in Fig. 3. The absence of saturation at 11 T is probably related to the non-favorable geometry of the nickel oxide: the highest angle between the $\{111\}$ planes and the xy plane occurs along the $[100]$ directions, i.e. at $\sim 54.7^\circ$. If we consider the projection and the saturation fields of Hoogeboom et al.¹⁷ (6 T) for single crystal, we expect a saturation field of 10.4 T, at the limit of the field range used.

From the measured SMR ratio $\Delta\rho/\rho$, we can set a lower limit for the spin mixing conductance by using the formula from the model based on spin diffusion theory by Chen et al.⁵

$$\frac{\Delta\rho}{\rho} = \theta_{SH}^2 \frac{\lambda}{d_{Pt}} Re \left(\frac{2\lambda G_{\uparrow\downarrow} \tanh^2\left(\frac{d_{Pt}}{2\lambda}\right)}{\sigma + 2\lambda G_{\uparrow\downarrow} \coth\left(\frac{d_{Pt}}{\lambda}\right)} \right) \quad (5)$$

where λ is the spin relaxation length in the Pt (1.1 nm),³¹ σ is the measured Pt conductivity ($5.5 \times 10^6 \Omega^{-1} \text{ m}^{-1}$), θ_{SH} is the spin Hall angle of the Pt (0.08),³¹ and d_{Pt} is the Pt thickness (7.5 nm). By using these values, we obtain the lower limit for the spin mixing conductance at the NiO/Pt interface to be $G_{\uparrow\downarrow} \sim 2 \times 10^{14} \Omega^{-1} \text{ m}^{-2}$. This value is compatible to what was obtained in YIG/Pt,⁴ and it fits well with the order of magnitude of recent theoretical predictions,⁷ while it is lower than what was reported by Han et al.¹⁵ in Pt/SrMnO₃. However, from the data by Hoogeboom et al.¹⁷ in single crystals of NiO(111)/Pt, where a strong dependence on the interface treatment was found, and considering that 11 T are not sufficient to saturate the signal, we expect that the spin mixing conductance can be further optimized.

In conclusion, we report on a negative spin Hall magnetoresistance in NiO(001)/Pt epitaxial thin films grown on MgO(001) substrates. The measured symmetry of the spin Hall magnetoresistance is consistent with theoretical expectations.⁷ Our results demonstrate that the SMR in epitaxial thin films is measurable even in the presence of clamping effect from a substrate and for crystal orientations not favorable for the magnetic moment reorientation in an easy plane. When the NiO(111) easy plane is not parallel to the surface of the NiO film, the redistribution of the magnetic domains as a function of the field is found to be non-trivial. We propose a simple model to determine the fraction of different S- domains, by taking into account the competition between Zeeman and destressing energy, for a thin film experiencing a clamping effect from the substrate. The model explains the quadratic field dependence of the SMR ratio, the negative sign of the SMR observed in the xy plane and the offset of the SMR in the yz plane, which is $\beta_{0,xx} = 31^\circ \pm 3^\circ$. From the observed SMR ratio, we estimated a spin mixing conductance greater than $2 \times 10^{14} \Omega^{-1} \text{ m}^{-2}$, close to the one observed in YIG/Pt.⁴ Our results confirm the potential of spin transport in antiferromagnetic insulating thin films, which are relevant for applications and represent a step toward the all-electrical detection of the magnetic moments in this class of materials.

Acknowledgements

This work was supported by Deutsche Forschungsgemeinschaft (DFG) SPP 1538 “Spin Caloric Transport,” the Graduate School of Excellence Materials Science in Mainz (MAINZ), and the EU project INSPIN (FP7-ICT-2013-X 612759). The authors acknowledge the support of SpinNet (DAAD Spintronics network, project number 56268455), MaHoJeRo (DAAD Spintronics network, project number 57334897), and the DFG (SFB TRR 173 SPIN+X). O.G. and J.S. acknowledge the Alexander von Humboldt Foundation and the ERC Synergy Grant SC2 (No. 610115). This work was supported by ERATO “Spin Quantum Rectification Project” (Grant No. JPMJER1402) and Grant-in-Aid for Scientific Research on Innovative Area, “Nano Spin Conversion Science” (Grant No. JP26103005) from JSPS KAKENHI, Japan, and the NEC Corporation. M.K. thanks ICC-IMR at Tohoku University for their hospitality during a visiting researcher stay at the Institute for Materials Research. The authors acknowledge useful scientific discussion with G. E. W. Bauer, R. Lebrun, D.-S. Han and K.-J. Lee, as well as skillful technical support from J. Henrizi.

References

- ¹ T. Jungwirth, X. Marti, P. Wadley, and J. Wunderlich, *Nat. Nanotechnol.* **11**, 231 (2016).
- ² V. Baltz, A. Manchon, M. Tsoi, T. Moriyama, T. Ono, and Y. Tserkovnyak, *arXiv:1606.04284* 1 (2016).
- ³ J. Sinova, S.O. Valenzuela, J. Wunderlich, C.H. Back, and T. Jungwirth, *Rev. Mod. Phys.* **87**, 1213 (2015).
- ⁴ H. Nakayama, M. Althammer, Y.T. Chen, K. Uchida, Y. Kajiwara, D. Kikuchi, T. Ohtani, S. Geprägs, M. Opel, S. Takahashi, R. Gross, G.E.W. Bauer, S.T.B. Goennenwein, and E. Saitoh, *Phys. Rev. Lett.* **110**, 206601 (2013).
- ⁵ Y.-T. Chen, S. Takahashi, H. Nakayama, M. Althammer, S.T.B. Goennenwein, E. Saitoh, and G.E.W. Bauer, *Phys. Rev. B* **87**, 144411 (2013).
- ⁶ E. V. Gomonaj and V.M. Loktev, *Phys. Rev. B* **64**, 64406 (2001).
- ⁷ A. Manchon, *Phys. Status Solidi - Rapid Res. Lett.* **11**, 1600409 (2017).
- ⁸ H. Ohldag, T.J. Regan, J. Stöhr, A. Scholl, F. Nolting, J. Lüning, C. Stamm, S. Anders, and R.L. White, *Phys. Rev. Lett.* **87**, 247201 (2001).
- ⁹ T. Shang, Q.F. Zhan, H.L. Yang, Z.H. Zuo, Y.L. Xie, L.P. Liu, S.L. Zhang, Y. Zhang, H.H. Li, B.M. Wang, Y.H. Wu, S. Zhang, and R.W. Li, *Appl. Phys. Lett.* **109**, 32410 (2016).
- ¹⁰ T. Shang, H.L. Yang, Q.F. Zhan, Z.H. Zuo, Y.L. Xie, L.P. Liu, S.L. Zhang, Y. Zhang, H.H. Li, B.M. Wang, Y.H. Wu, S. Zhang, and R.-W. Li, *J. Appl. Phys.* **120**, 133901 (2016).
- ¹¹ D. Hou, Z. Qiu, J. Barker, K. Sato, K. Yamamoto, S. Vélez, J.M. Gomez-Perez, L.E. Hueso, F. Casanova, and E. Saitoh, *Phys. Rev. Lett.* **118**, 147202 (2017).
- ¹² W. Lin and C.L. Chien, *Phys. Rev. Lett.* **118**, 67202 (2017).
- ¹³ Y.M. Hung, C. Hahn, H. Chang, M. Wu, H. Ohldag, and A.D. Kent, *AIP Adv.* **7**, 55903 (2017).
- ¹⁴ K. Ganzhorn, J. Barker, R. Schlitz, B.A. Piot, K. Ollefs, F. Guillou, F. Wilhelm, A. Rogalev, M. Opel, M. Althammer, S. Geprägs, H. Huebl, R. Gross, G.E.W. Bauer, and S.T.B.

- Goennenwein, Phys. Rev. B **94**, 94401 (2016).
- ¹⁵ J.H. Han, C. Song, F. Li, Y.Y. Wang, G.Y. Wang, Q.H. Yang, and F. Pan, Phys. Rev. B - Condens. Matter Mater. Phys. **90**, 144431 (2014).
- ¹⁶ O. Gomonay, S. Kondovych, and V. Loktev, J. Magn. Magn. Mater. **354**, 125 (2014).
- ¹⁷ G.R. Hoogeboom, A. Aqeel, T. Kuschel, T.T.M. Palstra, and B.J. van Wees, Appl. Phys. Lett. **111**, 52409 (2017).
- ¹⁸ O.L. Warren and P.A. Thiel, J. Chem. Phys. **100**, 659 (1994).
- ¹⁹ H. Gomonay and V.M. Loktev, J. Phys. Condens. Matter **14**, 3959 (2002).
- ²⁰ R.J. Powell and W.E. Spicer, Phys. Rev. B **2**, 2182 (1970).
- ²¹ W.L. Roth, J. Appl. Phys. **31**, 2000 (1960).
- ²² G.A. Slack, J. Appl. Phys. **31**, 1571 (1960).
- ²³ W.L. Roth and G.A. Slack, J. Appl. Phys. **31**, S352 (1960).
- ²⁴ J. Milano and M. Grimsditch, Phys. Rev. B - Condens. Matter Mater. Phys. **81**, 94415 (2010).
- ²⁵ J. Milano, L.B. Steren, and M. Grimsditch, Phys. Rev. Lett. **93**, 77601 (2004).
- ²⁶ F.L.A. Machado, P.R.T. Ribeiro, J. Holanda, R.L. Rodríguez-Suárez, A. Azevedo, and S.M. Rezende, Phys. Rev. B **95**, 104418 (2017).
- ²⁷ A.N. Bogdanov, A. V. Zhuravlev, and U.K. Röbber, Phys. Rev. B **75**, 94425 (2007).
- ²⁸ L. Baldrati, C. Schneider, T. Niizeki, R. Ramos, J. Cramer, A. Ross, E. Saitoh, and M. Kläui, Manuscript in Preparation (2017).
- ²⁹ M. Isasa, S. Vélez, E. Sagasta, A. Bedoya-Pinto, N. Dix, F. Sánchez, L.E. Hueso, J. Fontcuberta, and F. Casanova, Phys. Rev. Appl. **6**, 34007 (2016).
- ³⁰ T. Yamada, J. Phys. Soc. Japan **21**, 664 (1966).
- ³¹ N. Vlietstra, J. Shan, V. Castel, J. Ben Youssef, G.E.W. Bauer, and B.J. Van Wees, Appl. Phys. Lett. **103**, 32401 (2013).

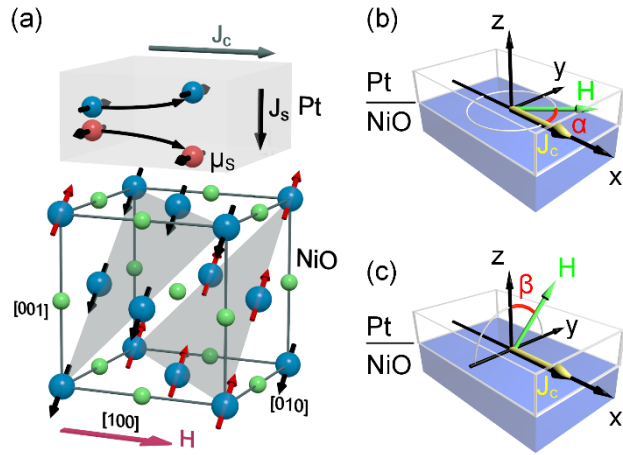


Fig. 1: (a) Measurement scheme of Spin Hall magnetoresistance (SMR) in MgO//NiO(001)/Pt. A charge current J_c flows in the Pt layer, yielding a transverse spin current J_s in the NiO, via the spin Hall effect. Depending on the relative orientation between the Néel vector \mathbf{N} and the current-induced spin polarization $\boldsymbol{\mu}_s$, the spin current is converted into an additional charge current by the inverse spin Hall effect, yielding the SMR. The spin structure of one of the twelve possible $(11\bar{2})$ S-domains of the NiO is shown, as well as the (111) easy plane. (b) Geometry of xy-plane magnetic field scans and definition of the angle α . (c) Geometry of xy-plane magnetic field scans and definition of the angle β .

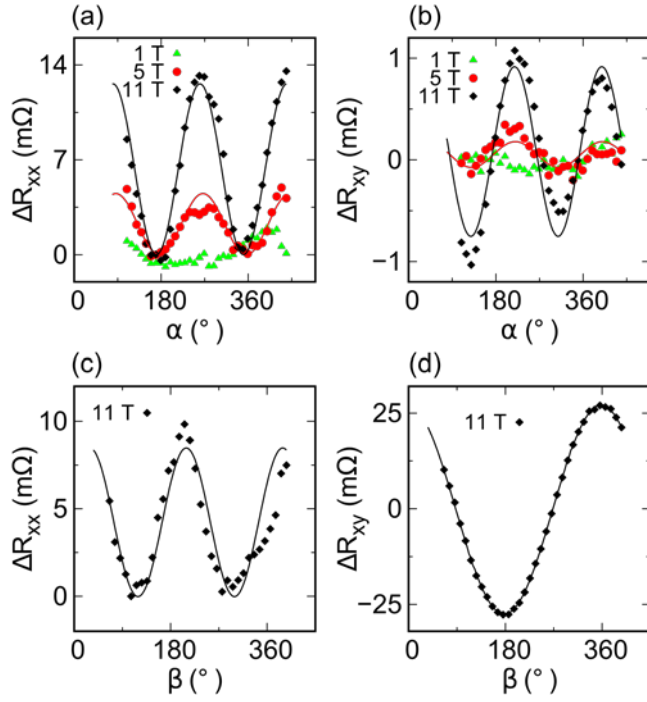


Fig. 2: Longitudinal ($\Delta R_{xx} = R_{xx}(\theta) - \min(R_{xx})$) and transverse ($\Delta R_{xy} = R_{xy}(\theta) - \bar{R}_{xy}$) angular dependence of the resistance variation of NiO/Pt bilayers at 199.46 ± 0.02 K. The angle θ indicates alternatively α or β angle, corresponding to the rotation in the xy or yz planes, respectively. The continuous lines are $\sin^2(\theta + \theta_0)$ or $\sin(\theta + \theta_0)$ fit of the data. (a) Longitudinal resistance variation ΔR_{xx} as a function of the in-plane angle α for an applied field of 1, 5 and 11 T. (b) Transverse resistance variation ΔR_{xy} as a function of the in-plane angle α . (c) Longitudinal resistance variation ΔR_{xx} as a function of the out-of-plane angle β . (d) Transverse resistance variation ΔR_{xy} as a function of the out-of-plane angle β , showing the predominance of the Hall effect.

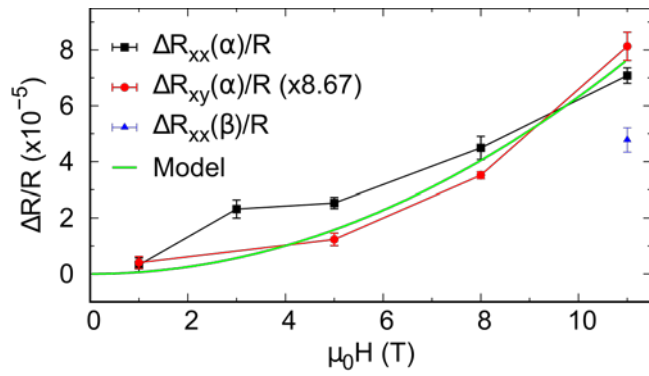


Fig. 3: Field dependence of the longitudinal and transverse SMR ratio in the xy- and yz- plane scans at 199.46 ± 0.02 K, compared to the theoretical model (green solid line). No saturation is observed in the field range used.